Novel View Synthesis from A Few Glimpses via Test-Time Natural Video Completion

Yan Xu¹ Yixing Wang¹ Stella X. Yu^{1,2}

¹University of Michigan

²UC Berkeley

{yxumich,yixingw,stellayu}@umich.edu

Abstract

Given just a few glimpses of a scene, can you imagine the movie playing out as the camera glides through it? That's the lens we take on *sparse-input novel view synthesis*, not only as filling spatial gaps between widely spaced views, but also as *completing a natural video* unfolding through space.

We recast the task as *test-time natural video completion*, using powerful priors from *pretrained video diffusion models* to hallucinate plausible in-between views. Our *zero-shot*, *generation-guided* framework produces pseudo views at novel camera poses, modulated by an *uncertainty-aware mechanism* for spatial coherence. These synthesized frames densify supervision for *3D Gaussian Splatting* (3D-GS) for scene reconstruction, especially in under-observed regions. An iterative feedback loop lets 3D geometry and 2D view synthesis inform each other, improving both the scene reconstruction and the generated views.

The result is coherent, high-fidelity renderings from sparse inputs without any scene-specific training or fine-tuning. On LLFF, DTU, DL3DV, and MipNeRF-360, our method significantly outperforms strong 3D-GS baselines under extreme sparsity. Our project page is at https://decayale.github.io/project/SV2CGS.

1 Introduction

Humans can effortlessly imagine how a scene appears from unseen viewpoints by mentally filling in gaps, by drawing on prior visual experience to infer what's missing. Inspired by this ability, we reinterpret novel view synthesis – a long-standing challenge in computer vision and graphics [8, 21, 11, 42, 31, 66, 44, 18, 27] – as the task of completing a natural video from sparse camera views (Fig. 1). From this perspective, sparse-input novel view synthesis becomes analogous to recovering missing frames in a video captured along an unconstrained camera trajectory. This framing naturally invites the use of powerful generative priors learned from large-scale video data. In particular, pretrained video diffusion models [5, 55], which are trained to synthesize coherent and realistic scene motions, offer a compelling tool for filling in plausible scene content between widely spaced views.

Recently, NeRF [31, 2, 4, 32] and 3D Gaussian Splatting (3D-GS) [18, 61, 13, 15, 28] have significantly advanced novel view synthesis. Unlike NeRF, which represents scenes using an implicit function, 3D-GS models scenes explicitly with a set of 3D Gaussian primitives and renders images through efficient rasterization. 3D-GS achieves photorealistic rendering with substantially faster inference speed, making it a focal point of recent research interest.

However, synthesis from sparse inputs remains difficult. NeRF or 3D-GS methods typically rely on dense input views to accurately constrain the optimization process. In sparse-view settings, occlusions and geometric ambiguities [63] often lead to rendering artifacts and degraded quality. Recent efforts [22, 67, 10, 16, 50, 52] focus more on constrained camera paths (e.g., object-centric or forward-facing views). In contrast, real-world image capture from walking with a handheld smartphone often produces widely spaced, unconstrained views with large occlusions and out-of-view regions (Fig. 1).

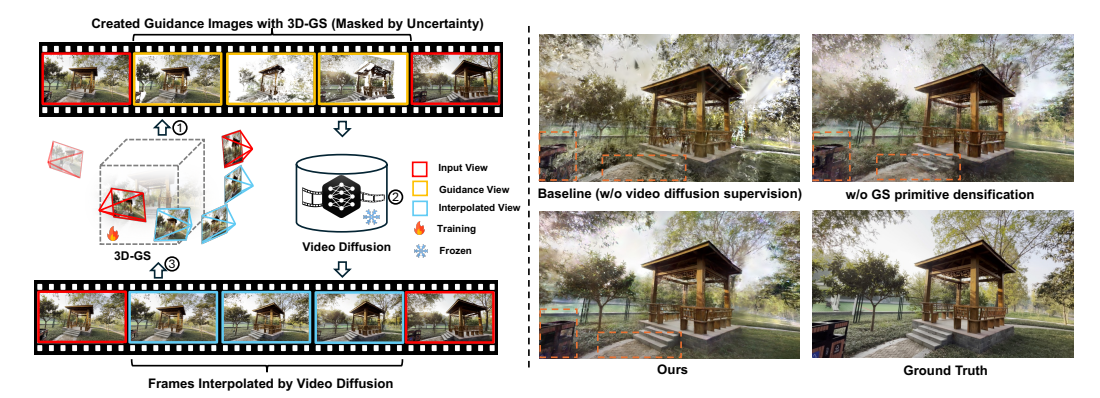


Figure 1: We view sparse-input novel view synthesis as temporal-spatial completion of a natural-looking video. **Left:** Our generation-guided reconstruction pipeline. With the initialized 3D-GS from sparse input views, ① we create guidance images on interpolated poses and estimate their uncertainty, based on the currently optimized 3D-GS. ② Using both guidance images and their uncertainties, we modulate the diffusion score function to interpolate between sparse input views. ③ The interpolated views are used to constrain 3D-GS optimization. **Right:** With our generation-guide reconstruction, the under-observed regions in the inputs are enhanced by the views generated by the diffusion model.

Motivated by the natural video completion perspective and strong priors in pretrained video diffusion models, we propose a **zero-shot**, **generation-guided reconstruction** pipeline integrating video diffusion with 3D-GS. Our approach defines target camera trajectories between sparse input views and uses video diffusion priors to synthesize plausible intermediate pseudo-views. These views provide supervision to better constrain 3D-GS training, especially in the under-observed regions in the inputs.

To recover missing views along a natural video trajectory, we must generate images at specified camera poses. However, existing video diffusion models [5, 6, 19, 45] are typically conditioned only on the initial frame and produce uncontrolled camera motions. While recent methods [49, 60] introduce trajectory conditioning during training, they still lack guarantees of pose alignment at inference and rely heavily on datasets with camera parameters, limiting generalization and scalability.

We propose a novel *uncertainty-aware modulation mechanism* that couples video diffusion with 3D Gaussian Splatting (3D-GS), enabling accurate, controllable frame interpolation under sparse-view settings. In this setup, 3D-GS provides a consistent 3D representation to guide view synthesis, while synthesized frames serve as pseudo supervision to further refine the 3D-GS model.

Fig. 1 illustrates our overall workflow. Our method begins by initializing 3D-GS from sparse views. After initialization, we interpolate camera poses between sparse inputs and create corresponding guidance images on the interpolated poses by inversely warping pixels from the nearest input view. The warping process is based on the depth maps rendered by the currently optimized 3D-GS. These guidance images are essential to maintaining the content and structural consistency during view interpolation, but may contain missing parts and artifacts due to imperfect 3D-GS depths and occlusion. We thus further model the uncertainty of these guidance images by assessing cross-view consistency in terms of photometry and geometry, and thereby focus the diffusion process more on correcting high-uncertainty regions, while keeping the reliable parts. Using both the guidance images and their associated uncertainties, we adaptively modulate the diffusion process to interpolate between the sparse views. The interpolated pseudo views are then added to the training set of 3D-GS. Furthermore, to improve the scene completeness for 3D-GS, we propose a *Gaussian primitive densification module* to densify the 3D-GS point cloud in under-observed regions using these pseudo views as bridges. The process above is repeated iteratively to refine the 3D-GS reconstruction.

To summarize, our contributions are threefold: 1) We propose a *zero-shot*, *generation-guided* 3D-GS pipeline that leverages pretrained video diffusion models to improve novel view synthesis under sparse inputs, particularly in under-observed regions. 2) We introduce an *uncertainty-aware modulation* mechanism to integrate 3D-GS with video diffusion for controllable pseudo-view generation, and a *Gaussian primitive densification* module to enhance scene completeness. 3) Our method achieves state-of-the-art performance, with over 2.5 dB PSNR gain on DL3DV and strong results on LLFF and DTU, demonstrating robust generalization. While we primarily use Stable Video Diffusion [5], our framework is agnostic to the diffusion backbone and compatible with alternatives [55, 19].

2 Related Work

Sparse-input Novel View Synthesis. Sparse-input novel view synthesis aims to reconstruct a representation for generating novel views of a scene using a few input images. Although existing training-based methods, *i.e.* NeRF [31] and 3DGS [18], work well with dense inputs, their performance drops significantly with sparse views due to overfitting [37, 46, 33, 12, 39]. Several recent works explore robust novel view synthesis under sparse inputs. One group [7, 33, 16, 43, 40, 20, 67, 56] focuses on imposing additional regularization on views deviating from the training views. For example, GeoAug [7] randomly samples novel views around input frames and constrains rendering to match the input after view warping. Niemeyer *et al.* [33] introduce smooth depth regularization on unseen views. SPARF [43], GeCoNeRF [20], and FewViewGS [56] integrate multi-view correspondence and geometry loss into optimization. However, these methods do not address the fundamental issue of information deficiency in unobserved regions.

Another line of methods explores including priors from pre-trained neural networks [12, 46, 51, 34, 67, 22] for regularization. For example, Jain *et al.* [16] leverage CLIP [36] features to provide semantic guidance. DSNeRF [12] and SparseNeRF [46] use depth regularization from pre-trained depth estimators on known views to guide optimization. More recently, FSGS [67] and DNGaussian [22] extend the similar sprit to 3D-GS training. However, these priors do not directly provide visual supervision for sparse-view NVS like the visual diffusion prior.

Novel View Synthesis with Diffusion Priors. To leverage visual priors for novel view synthesis, several lines of work have emerged. Liu *et al.* [26] use diffusion models to generate pseudo-observations at unseen views, while Wu *et al.* [50] guide the diffusion process using a NeRF representation [58] to synthesize novel views.

To reduce the computational burden of fine-tuning diffusion models, Xiong *et al.* [52] and Wang *et al.* [47] adopt Score Distillation Sampling (SDS) [35] to extract external visual priors. However, these approaches rely on image-based diffusion models and thus fail to fully capture spatiotemporal correlations across views. More recently, Liu *et al.* [25] fine-tuned Stable Video Diffusion [5] to provide view interpolation capability for guiding 3D-GS reconstruction. While this significantly improves performance, it requires substantial computational resources, limiting practical efficiency.

Despite progress in view-conditioned generative models [24, 48, 38, 62], existing methods are either object-centric [24] or struggle to generate photorealistic views [38, 62, 48]. Recent approaches [14, 57, 49, 60] enable coarse camera motion control for video generation from a single frame but lack a consistent 3D representation, which compromises cross-view consistency and reproducibility.

Consequently, how to effectively leverage zero-shot video diffusion priors for novel view synthesis is an important open challenge. The concurrent work [65] is closely related to ours, but it depends on a video diffusion model trained with camera poses [60], and the code was not publicly available at the time of our submission. In contrast, our method can, in principle, be applied to any video diffusion model trained on raw videos, making it more broadly generalizable.

3 Preliminaries – More Details in Appendix

3D Gaussian Splatting (3D-GS) [18] represents 3D scenes explicitly using Gaussian primitives, each defined by mean $\boldsymbol{\mu} \in \mathbb{R}^3$ and covariance $\boldsymbol{\Sigma} \in \mathbb{R}^{3 \times 3}$: $G(\boldsymbol{x}) = \exp\left(-\frac{1}{2}(\boldsymbol{x}-\boldsymbol{\mu})^{\top}\boldsymbol{\Sigma}^{-1}(\boldsymbol{x}-\boldsymbol{\mu})\right)$. Each Gaussian also includes spherical harmonics coefficients \boldsymbol{c} for view-dependent color and an opacity α , enabling expressive appearance modeling. Rendering is performed efficiently via rasterization. After projecting Gaussians to the image plane, pixel colors are computed using alpha compositing: $C_{\text{pix}} = \sum_i c_i \alpha_i \prod_{j=1}^{i-1} (1-\alpha_j)$, where c_i and α_i denote the color and opacity of the i-th Gaussian, respectively. For depth rendering, c_i is replaced by the z-buffer value.

Stable Video Diffusion (SVD) [5] is an image-to-video diffusion model that generates natural video conditioned on an input image. By default, generation starts from the given image and autonomously evolves, incorporating random camera movements and scene dynamics.

Given a forward diffusion process expressed by $d\mathbf{x} = f(t)\mathbf{x}dt + g(t)d\mathbf{w}$, where \mathbf{x} is the noisy latent state at timestamp t, \mathbf{w} denotes the standard Wiener process, and f(t) and g(t) are scalar functions, its reverse process ODE [41] can be expressed as $d\mathbf{x} = \left[f(t)\mathbf{x} - \frac{1}{2}g^2(\mathbf{x})\nabla_{\mathbf{x}}\log(q_t(\mathbf{x}))\right]dt$. In the case of the variance exploding (VE) diffusion [41] adopted by Stable Video Diffusion (SVD) [5], it

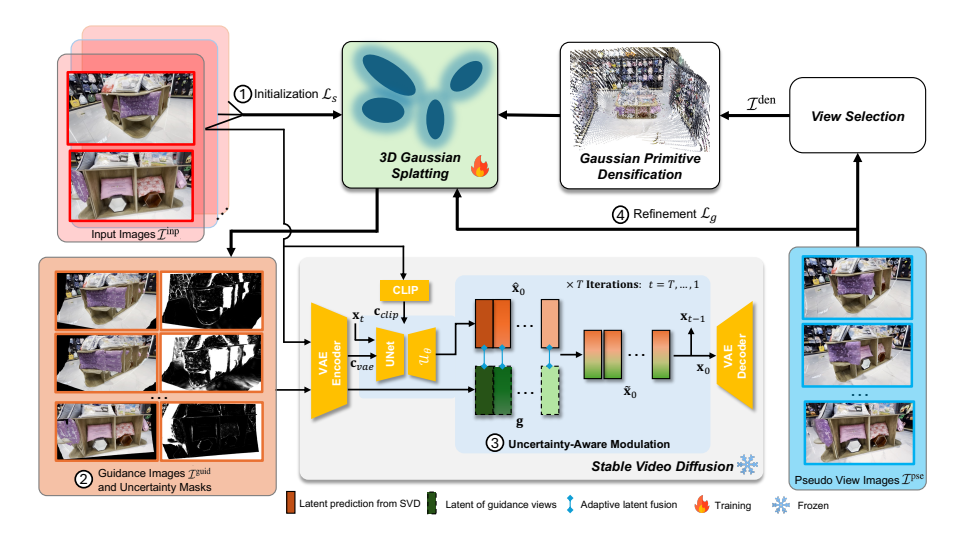


Figure 2: **Overall framework**. After initializing 3D-GS from sparse input images (①), ② we create guidance images (Sec. 4.1.1) and assess their uncertainties (Sec. 4.1.2) based on the current 3D-GS renderings. ③ The guidance images guide the diffusion process through the uncertainty-aware modulation (Sec. 4.1.3). The diffusion process enhances high-uncertain regions while preserving reliable parts. ④ The generated pseudo-view images are then used to densify the Gaussian primitives (Sec. 4.2.1) and to constrain the 3D-GS training (Sec. 4.2.2). For illustration, we show pseudo-view generation from one image pair, though all pairs are processed sequentially in practice.

can be simplified as: $d\mathbf{x} = \frac{\mathbf{x} - \hat{\mathbf{x}}_0}{\sigma_t} d\sigma_t$, where the noise of the diffusion process is parameterized as Gaussian noise with a variance of σ_t and $\hat{\mathbf{x}}_0$ is the currently predicted clean video by the network based on the latent state at the previous step. In practice, we can obtain the estimated denoised sample \mathbf{x}_{t-1} at the previous time step by discretizing the diffusion process above:

$$\mathbf{x}_{t-1} = \mathbf{x}_t + \frac{\mathbf{x}_t - \hat{\mathbf{x}}_0}{\sigma_t} (\sigma_{t-1} - \sigma_t). \tag{1}$$

4 Our Test-Time Optimization Approach to Novel View Synthesis

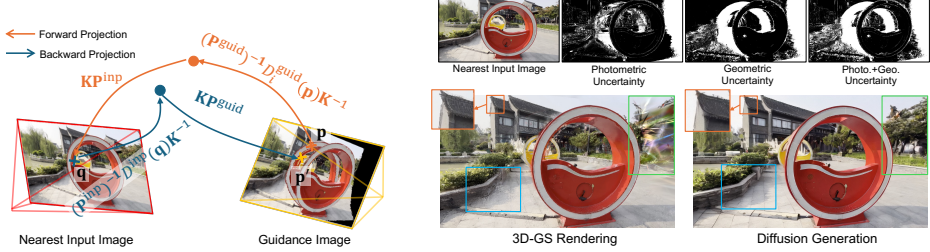
We recast sparse-input novel view synthesis as a test-time natural video completion problem. To this end, we propose an iterative optimization framework that integrates 3D Gaussian Splatting with video diffusion priors to enforce geometric consistency and enhance visual fidelity.

Given a few input views \mathcal{I}^{inp} and their associated camera poses, we propose a zero-shot, generation-guided reconstruction pipeline that synthesizes novel views by leveraging a pretrained video diffusion model [5] (Fig. 2). The framework consists of four main steps: 1) **3D-GS initialization** from the sparse input views; **2) Guidance feature creation** (Sec. 4.1.1) and their **uncertainty estimation** via a cross-view consistency check(Sec. 4.1.2) based on the current 3D-GS; **3) Uncertainty-aware modulation** of the video diffusion model in generating pseudo views, conditioned on the guidance images and uncertainty masks (Sec. 4.1.3); **4) Refinement of the 3D-GS** by densifying the Gaussian primitives using the generated pseudo-views (Sec. 4.2). Steps **2)-4**) are iteratively performed to progressively improve both the 3D-GS representation and the quality of the diffusion model outputs.

4.1 Pseudo View Generation via Uncertainty-Aware Modulation

Most off-the-shelf video diffusion models lack precise camera control due to the scarcity of datasets with known camera poses. To ensure broad applicability, we design our framework to be compatible with widely available models [5, 55] that are conditioned solely on a single image. Moreover, our approach is theoretically agnostic to variance-exploding diffusion backbones [41].

The modern video diffusion model [5] usually extracts CLIP [36] features \mathbf{c}_{clip} from the input frame I^{inp} to inform the U-Net of the scene's overall appearance and layout. Simultaneously, the frame is encoded by a VAE encoder to produce contextual features \mathbf{c}_{vae} , which are injected via classifier-free



(a) Illustration of Forward/Backward Projection (b) Example of the Uncertainty Estimates

Figure 3: Cross-view consistency is evaluated through the forward and backward projections shown in (a) to estimate the uncertainty of the generated guidance image. As illustrated in (b), regions exhibiting poor cross-view consistency (regions in the boxes) are identified as high-uncertainty areas (brighter), which are subsequently refined by the video diffusion model.

guidance to maintain consistency with the reference frame. At each denoising timestep t, the model denoises a latent video representation $\mathbf{x}_t \in \mathbb{R}^{N \times C \times H \times W}$ using a U-Net $\mathcal{U}_{\theta}(\mathbf{x}_t; \mathbf{c}_{\text{clip}}, \mathbf{c}_{\text{vae}}, t)$, where N, C, H, W are the number of frames, feature and spatial dimensions of the latent, respectively. The U-Net predicts a clean latent $\hat{\mathbf{x}}_0$ from \mathbf{x}_t to update \mathbf{x}_t with Eq. (1), which direct \mathbf{x}_t toward $\hat{\mathbf{x}}_0$. The final denoised latent, \mathbf{x}_0 , is decoded by the VAE decoder into a video clip.

Our method draws inspiration from diffusion-based image editing techniques [29, 59, 1, 53], particularly SDEdit [29] for its efficiency. Specifically, we propose to modify the original clean latent prediction $\hat{\mathbf{x}}_0$ using the guidance feature $\mathbf{g} \in \mathbb{R}^{N \times C \times H \times W}$ extracted from the guidance images by the VAE encoder. This modification is formulated as an optimization problem applied to each frame i:

$$\widetilde{\mathbf{x}}_0[i] = \underset{\mathbf{x}}{\operatorname{arg min}} \|\mathbf{x} - \hat{\mathbf{x}}_0[i]\|_2^2 + \gamma_{t,i} \|\mathbf{x} - \mathbf{g}[i]\|_2^2, \tag{2}$$

where index [i] denotes the i-th frame channel corresponding to the i-th frame of the generated video, and $\gamma_{t,i} > 0$ is a weighting term that controls the influence of the guidance feature.

The remaining problems are 1) how to get the proper feature map g to guide the diffusion model in generating views of desired poses (Sec. 4.1.1) and 2) how to control $\gamma_{t,i}$ to achieve adaptive modulation (Sec. 4.1.2-4.1.3).

4.1.1 Guidance Feature Creation

The core idea of our approach is to exploit video diffusion priors to infer occluded or missing content from sparse input views. This requires constructing guidance features that are geometrically aligned with the desired target view. To this end, a simple strategy is to render the target views from the current 3D-GS and encode them with the diffusion model's VAE encoder, thereby maintaining 3D consistency. However, this often yields low-fidelity results, as 3D-GS may produce inaccurate color renderings at novel poses during training.

To resolve this, instead of using the 3D-GS to render color images, we create guidance images by inversely warping pixels from their nearest input view, using depth maps rendered by 3D-GS. Concretely, to construct the guidance image $I_i^{\rm guid}$ for the i-th video frame, we first project each pixel $\mathbf{p} \in I^{\rm guid}$ into the nearest input view $I^{\rm inp} \in \mathcal{I}^{\rm inp}$, using the rendered depth map $D_i^{\rm guid}$, camera intrinsics \mathbf{K} , and camera poses $\mathbf{P}^{\rm inp} \in \mathbb{SE}(3)$ (input view) and $\mathbf{P}_i^{\rm guid} \in \mathbb{SE}(3)$ (guidance view), to get its corresponding pixel \mathbf{q} in the input image:

$$\mathbf{q} = \mathbf{K} \mathbf{P}^{\text{inp}} (\mathbf{P}_i^{\text{guid}})^{-1} D_i^{\text{guid}} (\mathbf{p}) \mathbf{K}^{-1} \mathbf{p}.$$
(3)

We fill pixel $\mathbf p$ with the color of pixel $\mathbf q$ to obtain the guidance image I_i^{guid} . The set of guidance images is denoted as $\mathcal I^{\mathrm{guid}} = \{I_i^{\mathrm{guid}}\}_{i=1}^N$, where N is the length of the video clip generated by the video diffusion model in a single pass. The VAE encoder will encode these guidance images to have the corresponding guidance feature maps $\mathbf g$ to guide the diffusion process via Eq. (2).

4.1.2 Uncertainty Evaluation from Cross-View Consistency

The constructed guidance images well preserve scene content and structure by adhering to strict multi-view geometric constraints imposed by the 3D-GS representation. However, because 3D-GS is

imperfect during training, especially in under-observed regions, the guidance images may contain missing content or artifacts. To assess the reliability of guidance images, we introduce a strict cyclic consistency check, as illustrated in Fig. 3a. Specifically, in the forward pass, we project each pixel \mathbf{p} in the guidance image to its corresponding pixel \mathbf{q} in the nearest input image using Eq. (3). We then perform a backward projection from \mathbf{q} to the guidance view using the depth map D^{inp} rendered by 3D-GS from the nearest input view: $\mathbf{p'} = \mathbf{KP}_i^{\text{guid}}(\mathbf{P}^{\text{inp}})^{-1}D^{\text{inp}}(\mathbf{q})\mathbf{K}^{-1}\mathbf{q}$. The uncertainty at pixel \mathbf{p} is then quantified by evaluating both geometric and photometric consistency:

$$U_i(\mathbf{p}) = 1 - \exp\left(-\frac{||\mathbf{p} - \mathbf{p}'||_2^2}{s_1} - \frac{||I_i^{gs}(\mathbf{p}) - I^{inp}(\mathbf{q})||_2^2}{s_2}\right),\tag{4}$$

where $I_i^{\rm gs}$ is the 3D-GS rendered image from the view of the *i*-th guidance image, $I^{\rm inp}$ denotes the nearest input image, and s_1 , s_2 are bandwidth parameters controlling the sensitivity to geometric and photometric discrepancies. If the 3D-GS is well constrained at pixel **p** and no occlusion is present, the image pixel color $I^{\rm inp}(\mathbf{q})$ should closely match the color of the 3D-GS rendering $I_i^{\rm gs}(\mathbf{p})$, and the back-projected position \mathbf{p}' should lie near the original \mathbf{p} . This results in low uncertainty. Otherwise, discrepancies in color or geometry increase the uncertainty, as captured by Eq. (4).

4.1.3 Uncertainty-Aware Modulation

Using the uncertainty map, we define $\gamma_{t,i}$ for each pixel in Eq. (2) as:

$$\gamma_{t,i}(\mathbf{p}) = \begin{cases} 0 & U_i(\mathbf{p}) > \delta \text{ or } t < \tau \\ 1/(U_i(\mathbf{p}) + \epsilon) & \text{otherwise} \end{cases}$$
(5)

where δ and τ are threshold hyperparameters and ϵ is a small constant to avoid division by zero. The threshold τ is determined by the overall uncertainty of frame i, measured by $\tau = \frac{k}{HW} \sum_{\mathbf{p}} (U_i(\mathbf{p})) + b$, with k and b as tunable coefficients. This ensures that in uncertain regions, the optimization in Eq. (2) leans towards the diffusion prediction $\hat{\mathbf{x}}_0[i]$, while reliable areas are guided by the features from $\mathbf{g}[i]$. For simplicity, we let \mathbf{p} denote corresponding positions in both image and latent space. In practice, U_i is downsampled via average pooling to match the latent resolution before computing $\gamma_{t,i}$. After computing $\gamma_{t,i}$, we apply Eq. (2) to obtain the fused latent $\widetilde{\mathbf{x}}_0[i]$, which is then used in Eq. (1) to update \mathbf{x}_t to \mathbf{x}_{t-1} . This reverse sampling step is repeated until the final latent \mathbf{x}_0 is obtained, which is then decoded into pseudo-view images via the VAE decoder (see Fig. 2).

4.1.4 Extending to View Interpolation

The above generation pipeline supports view extrapolation from a single input, but may struggle to preserve scene fidelity under large viewpoint shifts. To alleviate this issue, we extend it to view interpolation using two input views as references. We define camera trajectories between them and run the diffusion model forward and backward, conditioned on the start and end images, respectively. At each denoising step, we merge the two latent sequences $\mathbf{x}_{t-1} := \beta \mathbf{x}_{t-1}^{\text{forward}} + (1-\beta)R(\mathbf{x}_{t-1}^{\text{backward}})$, where $R(\cdot)$ is the reverse operation along the frame index dimension to align the latent $\mathbf{x}_{t-1}^{\text{backward}}$ to $\mathbf{x}_{t-1}^{\text{forward}}$ in the frame dimension. $\beta \in \mathbb{R}^N$ is the blending weight, with $\beta[i] = (N-i)/(N-1)$ for $i=1,2,\ldots,N$, where N is number of interpolated frames between two inputs. See supplementary material for the detailed algorithm.

4.2 3D-GS Optimization Guided by Generation

To constrain the 3D-GS representation, we generate pseudo views by pairing adjacent input images and defining camera trajectories that better cover under-observed regions (see supplementary materials for details). Using the video diffusion model guided by the generated guidance images $\mathcal{I}^{\mathrm{guid}}$, as described in Sec. 4.1, we interpolate between input views to obtain pseudo-view images $\mathcal{I}^{\mathrm{pse}} = \{I_j^{\mathrm{pse}}\}_{j=1}^{pN}$, where p is the number of input image pairs.

4.2.1 Gaussian Primitive Densification

Sparse-input 3D-GS training often yields poor reconstruction in under-observed regions due to limited supervision. To mitigate this, we enhance 3D-GS geometry using generated pseudo-views \mathcal{I}^{pse} and a dense stereo model [48]. For efficiency, we select a subset of pseudo-views $\mathcal{I}^{den} \subseteq \mathcal{I}^{pse}$ whose camera poses yield low inter-frame covisibility, ensuring broad scene coverage with minimal redundancy. These views are used to build a camera graph and optimize a point cloud from stereo predictions. To further improve robustness, we analyze the spatial distribution of the reconstructed points and filter

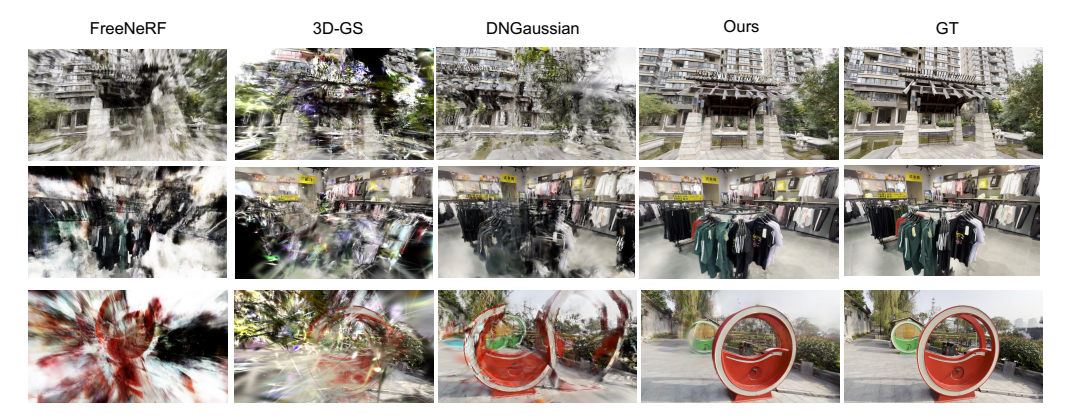


Figure 4: **Qualitative comparison with existing methods on the DL3DV dataset** demonstrates the robustness of our methods against sparse inputs. Leveraging the priors of the video diffusion model, our method renders photorealistic novel views from only 9 input views, while other methods produce noisier, less realistic results.

out those that significantly deviate from the global average distance to neighboring points. Finally, we query existing Gaussian primitives within a fixed radius of each remaining point and only add new Gaussian primitives at positions without nearby primitives to augment the current set. See appendix for more details.

4.2.2 3D Gaussian Splatting Optimization

After densifying the Gaussian primitive set, we optimize the 3D-GS model using both the original inputs and the generated pseudo-views. In each training iteration, one input view and one pseudo-view are sampled for supervision. For the original input views, we apply an L1 loss and a D-SSIM loss , as well as a depth regularization term \mathcal{L}_{reg} with Pearson correlation similar to [47]: $\mathcal{L}_s = w_1 \mathcal{L}_1(I^{\text{gs}}, I^{\text{inp}}) + w_2 \mathcal{L}_{\text{D-SSIM}}(I^{\text{gs}}, I^{\text{inp}}) + w_3 \mathcal{L}_{\text{reg}}$, where I^{gs} is the rendered image from 3D-GS and I^{inp} denotes the corresponding input image. For the generated pseudo views, we observe that, despite the carefully designed guidance mechanism, some regions still suffer from temporal inconsistency—particularly distant areas with weak geometry or those with fine-grained textures, e.g., grass or tree leaves. To mitigate the negative impact of such inconsistencies on 3D-GS training, we use the LPIPS loss [64] instead of L1 loss. The resulting loss for pseudo-views is:

$$\mathcal{L}_g = w_4 \mathcal{L}_{\text{LPIPS}}(I^{\text{gs}}, I^{\text{pse}}) + w_5 \mathcal{L}_{\text{D-SSIM}}(I^{\text{gs}}, I^{\text{pse}}) + w_6 \mathcal{L}_{\text{reg}}.$$
 (6)

5 Experiments

5.1 Experiment Settings

Datasets and Metrics. We evaluate our method on LLFF [30], DL3DV [23], DTU [17], and MipNeRF-360 [3] datasets. LLFF consists of 8 forward-facing scenes. Following standard practice [54, 22], we train our model using only 3 input views on this dataset. DL3DV comprises diverse indoor and outdoor scenes, captured by humans walking through scenes. The Mip-NeRF 360 dataset consists of real-world indoor and outdoor scenes designed for evaluating novel view synthesis in large, unbounded environments. Compared to LLFF, DTU, and Mip-NeRF 360, DL3DV offers more diverse scene types and exhibits significantly more complex and dynamic camera motions. We include this dataset to evaluate the robustness of our approach under more realistic and challenging conditions, and our evaluation is conducted on the official test split of DL3DV. To verify the generalizability of our methods and compare with the previous methods, we also test our methods on DTU, an object-centric dataset captured in controlled conditions. For the DTU dataset, we follow the protocol from RegNeRF [22], using 3 training views (IDs 25, 22, and 28) across 15 evaluation scenes. To focus on the object of interest, we mask out the background during evaluation using the provided object masks, consistent with [54, 22]. We apply a downsampling factor of 8 for LLFF and 4 for DTU, aligning with prior work. The rendering quality is assessed using PSNR, SSIM, and LPIPS metrics.

Implementation details. Our pipeline is designed to operate iteratively. In each cycle, we train the 3D-GS model for 10K iterations, followed by an update of the pseudo-view images using the video

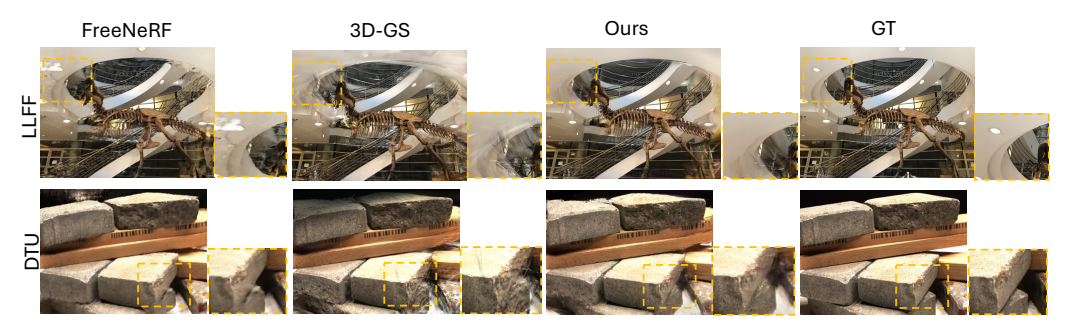


Figure 5: Qualitative comparison with other methods on DTU and LLFF datasets.

Table 1: Quantitative comparisons with other methods on LLFF, DTU, and MipNeRF-360 demonstrate our state-of-the-art performance and strong generalization ability. Left: Quantitative comparison with other methods on the LLFF dataset with 3 training views. Middle: Comparison on the DTU dataset with 3 training views. Right: Comparison on the MipNeRF-360 dataset with 9 training views. Recent reconstruction-based methods, feed-forward methods, and non-zero-shot methods are included. We color each cell as best , second best , and third best .

LLFF	PSNR↑	SSIM↑	LPIPS↓	DTU	PSNR↑	SSIM↑	LPIPS				
Mip-NeRF [2]	16.11	0.401	0.460	Mip-NeRF [2]	8.68	0.571	0.353	MipNeRF-360	PSNR↑	SSIM↑	LPIPS↓
3D-GS [18]	17.43	0.522	0.321	3D-GS [18]	10.99	0.571	0.333	RegNeRF [33]	13.73	0.193	0.629
DietNeRF [16]	14.94	0.370	0.496	DietNeRF [16]	11.85	0.633	0.314	FreeNeRF [54]	13.20	0.198	0.635
RegNeRF [33]	19.08	0.587	0.336	RegNeRF [33]	18.89	0.745	0.190	DNGaussian [22]	12.51	0.228	0.683
FreeNeRF [54]	19.63	0.612	0.308	FreeNeRF [54]	19.92	0.787	0.182	MVSplat 360 [9]	14.86	0.321	0.528
SparseNeRF [46] FSGS [67]	19.86	0.624	0.328	SparseNeRF [46]	19.55	0.769	0.201	ViewCrafter [60]	16.68	0.382	0.551
DNGaussian [22]	19.12	0.632	0.288	DNGaussian [22]	18.91	0.790	0.176	3DGS-Enhancer [25]	16.22	0.399	0.454
IPSM [47]	20.44	0.702	0.294	SparseGS [52]	18.89	0.834	0.178	Ours	17.91	0.495	0.435
Ours	20.44	0.702	0.207	Ours	20.51	0.840	0.137				
Ours	20.01	0.705	0.201								

diffusion model. After each pseudo-view update, we reset the learning rate schedule of 3D-GS before starting the next optimization cycle to avoid overfitting. For the uncertainty estimation in Eq. (4), we set the bandwidth parameters to $s_1=100$ and $s_2=0.25$. The δ in Eq. (5) is fixed at 0.5 across all experiments. The loss weights are configured as follows: $w_1=0.8, w_2=0.2, w_3=1.0, w_4=1.0, w_5=0.2$, and $w_6=1.0$. Additional implementation details are provided in supplementary materials.

5.2 Comparison with Other Methods

We compare our method against state-of-the-art approaches on four benchmark datasets to demonstrate its effectiveness and generalizability across diverse scenarios.

Comparison on LLFF. We evaluate our method on the LLFF dataset captured by a swaying face-forward camera. As shown in Table 1 (left), our method consistently outperforms NeRF-based approaches across all evaluation metrics. When compared to 3D-wGaussian Splatting-based baselines such as FSGS [67] and DNGaussian [22], our method remains competitive, particularly in LPIPS and SSIM scores. This improvement is largely attributed to the additional supervisory signal provided by the pseudo views generated through the video diffusion model. Notably, the LPIPS metric, which correlates more closely with human perceptual similarity than traditional metrics like PSNR, highlights our method's ability to produce visually realistic novel views. Qualitative comparisons are presented in Fig. 5.

Comparison on DTU. To further assess the generalizability of our approach, we evaluate and compare its performance on the DTU dataset. DTU is an object-centric dataset in which each scene contains a centered object against a monotone background. The evaluation results are presented in Table 1 (middle). In this setting, our method still performs well and outperforms other NeRF-based and 3D-GS-based methods. Specifically, our method outperforms the second-best approach by a significant margin in terms of PSNR, SSIM, and LPIPS. While NeRF-based methods also exhibit competitive accuracy in this scenario, they suffer from slow rendering speeds (approximately 0.21 FPS), whereas our 3D-GS-based approach supports real-time rendering at around 430 FPS.

Comparison on DL3DV. We compare with other cutting-edge counterparts on the DL3DV dataset under 3,6, and 9 view settings. Table 2 shows the quantitative comparison results. Apart from the sparse-input 3D-GS methods, we also compare with the non-sparse view methods and NeRF-based methods in Table 2. We outperform previous state-of-the-art methods [22, 67, 47] by a significant

Table 2: Our method outperforms other test-time optimization methods on the DL3DV dataset. The results are reported for 3, 6, and 9 training views. We color each cell as **best**, **second best**, and **third best**.

	3 Views			6 Views			9 Views		
Method	PSNR↑	SSIM↑	LPIPS↓	PSNR↑	SSIM↑	LPIPS↓	PSNR↑	SSIM↑	LPIPS↓
Mip-NeRF [2]	10.92	0.191	0.618	11.56	0.199	0.608	12.42	0.218	0.600
3DGS [18]	10.97	0.248	0.567	12.34	0.332	0.598	12.99	0.403	0.546
RegNeRF [33]	11.46	0.214	0.600	12.69	0.236	0.579	12.33	0.219	0.598
FreeNeRF [54]	10.91	0.211	0.595	12.13	0.230	0.576	12.85	0.241	0.573
FSGS [67]	12.22	0.296	0.535	13.73	0.429	0.540	15.52	0.468	0.416
DNGaussian [22]	11.10	0.273	0.579	12.67	0.329	0.547	13.44	0.365	0.539
IPSM [47]	11.70	0.279	0.534	12.82	0.332	0.521	13.41	0.361	0.529
Ours	14.62	0.471	0.491	17.35	0.566	0.396	19.19	0.616	0.335

Table 3: **Ablation experiments on the DL3DV test set**. (a) Experiments to show the effectiveness of the proposed components in pseudo-view generation step. (b) Experiments to show the effectiveness of the proposed strategies for 3D-GS optimization.

(a)	PSNR↑	$SSIM \!\!\uparrow$	LPIPS↓
Baseline 3D-GS	16.59	0.502	0.405
w/ GS interpolation	18.59	0.591	0.369
w/ warping interpolation (full)	19.19	0.616	0.335
w/o geometric	18.21	0.583	0.378
w/o photometric	18.93	0.612	0.352

(b)	PSNR↑	SSIM↑	LPIPS↓
w/o point filtering	19.01	0.615	0.343
w/o GS densification	18.23	0.567	0.386
w/o LPIPS loss	18.81	0.597	0.351
Full model	19.19	0.616	0.335

margin in this challenging setting. We observe that although DNGaussian [22] works well in environments with limited scope or with limited camera motions, *e.g.*, object-centric scenarios, it has difficulties in reliably reconstructing the open environment due to the lack of constraints in under-observed regions, as the sparse (a qualitative results shown in Fig. 4). Similarly, FSGS [67] also struggles in this challenging setting, though it achieves slightly better performance compared with DNGaussian because it uses a sparse point cloud for initialization. The recent work IPSM [47] uses an image diffusion model to constrain the 3D-GS by enhancing Score Distillation Sampling (SDS). As shown in Table 2, this method struggles with extremely sparse inputs. This limitation arises because the image diffusion model lacks access to a global scene context, whereas the video diffusion model is able to infer such context from the input reference frame.

Comparison on MipNeRF-360. To evaluate our method on unbounded scenes and ensure a fair comparison with recent feed-forward approaches [9, 60, 25], we further conduct experiments on the Mip-NeRF 360 dataset [3]. Our method consistently outperforms reconstruction-based methods [33, 54, 22] and surpasses state-of-the-art feed-forward approaches [9, 60, 25] by a notable margin. As shown in Fig. 6, although feed-forward methods can hallucinate novel views from sparse inputs through large-scale data training, they often struggle to maintain geometric consistency, fine details, and color fidelity compared to our approach.

5.3 Ablation Study

To validate the effectiveness of our proposed components in the pseudo view generation (Sec. 4.1) and the 3D-GS optimization (Sec. 4.2), we conduct an extensive ablation study on DL3DV.



Figure 6: Our test-time optimization better preserves visual and geometric consistency than the feed-forward approach, MVSplat360. While feed-forward methods can produce plausible novel views, they often struggle to maintain fidelity to the original scene, whereas our method achieves higher consistency.

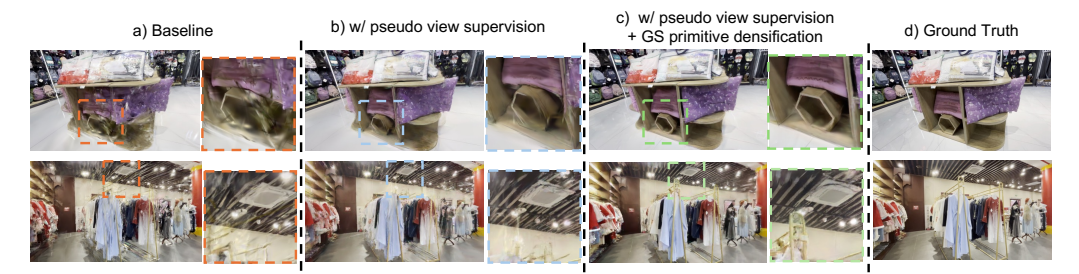


Figure 7: The proposed pseudo-view supervision and primitive densification effectively enhance the novel view synthesis, especially in under-observed regions from the inputs. Zoom in for a better view.



Figure 8: The estimated uncertainty mask identifies the unreliable parts in guidance images. The video diffusion model cannot generate faithful images without involving the uncertainty mask.

Effectiveness of uncertainty-aware modulation mechanism. Table 3a compares the baseline 3D-GS trained on sparse views using \mathcal{L}_s with two variants: one using 3D-GS renderings as guidance ("w/ GS interpolation") and one using our warping-based guidance ("w/ warping interpolation"). While GS interpolation improves over the baseline, it underperforms compared to our method due to inaccurate color rendering at novel poses during training.

Fig. 8 shows the effect of uncertainty-aware modulation by comparing diffusion results with and without it, using identical guidance images. We further ablate the geometric and photometric terms in the uncertainty formulation (Eq. (4)), denoted as "w/o geometric" and "w/o photometric." As shown in Table 3a, removing either term noticeably degrades performance.

Effectiveness of Gaussian primitive densification. We ablate the densification step ("w/o GS densification" in Table 3b), observing a significant performance drop, highlighting its role in improving synthesis quality. Fig. 7 shows that densification enhances reconstruction in under-observed regions. Removing the point filtering step ("w/o point filtering") also degrades performance due to depth outliers from the stereo model.

Effectiveness of LPIPS for pseudo view supervision. We replace LPIPS with L1 loss ("w/o LPIPS loss") in Eq. (6), observing a notable performance drop (Table 3b). Despite our guidance strategy, cross-view inconsistencies – especially in distant or textured regions – remain challenging. L1 loss used in vanilla 3D-GS [18] is less robust to such inconsistencies in diffusion-generated pseudo views.

6 Conclusion and Limitation

We introduced a zero-shot, generation-guided pipeline that leverages a pretrained video diffusion model to improve 3D-GS reconstruction from sparse inputs. Intermediate views are synthesized and guided by warped depth-based images and uncertainty-aware modulation. A densification module further enhances scene completeness. Our approach improves photorealism and coverage in sparse settings while maintaining the real-time efficiency of 3D-GS.

Our framework improves sparse-view synthesis but has limitations. It depends on the quality of the pretrained video diffusion model, which may introduce artifacts under extreme views or complex scenes. Iterative training adds overhead compared with vanilla 3D-GS pipelines, and early 3D-GS depth errors can affect guidance quality despite uncertainty modeling, though this impact typically decreases over time.

Societal Impact. This technology can benefit AR/VR, robotics, digital content creation, telepresence, and cultural heritage preservation. However, its computational demands may contribute to a higher carbon footprint.

Acknowledgment. This project was supported, in part, by NSF 2215542, NSF 2313151, and Bosch gift funds to S. Yu at UC Berkeley and the University of Michigan.

References

- [1] Arpit Bansal, Hong-Min Chu, Avi Schwarzschild, Soumyadip Sengupta, Micah Goldblum, Jonas Geiping, and Tom Goldstein. Universal guidance for diffusion models. In *Proceedings of the IEEE/CVF Conference on Computer Vision and Pattern Recognition*, pages 843–852, 2023.
- [2] Jonathan T Barron, Ben Mildenhall, Matthew Tancik, Peter Hedman, Ricardo Martin-Brualla, and Pratul P Srinivasan. Mip-nerf: A multiscale representation for anti-aliasing neural radiance fields supplemental material.
- [3] Jonathan T Barron, Ben Mildenhall, Dor Verbin, Pratul P Srinivasan, and Peter Hedman. Mip-nerf 360: Unbounded anti-aliased neural radiance fields. In *Proceedings of the IEEE/CVF conference on computer vision and pattern recognition*, pages 5470–5479, 2022.
- [4] Jonathan T Barron, Ben Mildenhall, Dor Verbin, Pratul P Srinivasan, and Peter Hedman. Zip-nerf: Anti-aliased grid-based neural radiance fields. In *Proceedings of the IEEE/CVF International Conference on Computer Vision*, pages 19697–19705, 2023.
- [5] Andreas Blattmann, Tim Dockhorn, Sumith Kulal, Daniel Mendelevitch, Maciej Kilian, Dominik Lorenz, Yam Levi, Zion English, Vikram Voleti, Adam Letts, et al. Stable video diffusion: Scaling latent video diffusion models to large datasets. arXiv preprint arXiv:2311.15127, 2023.
- [6] Andreas Blattmann, Robin Rombach, Huan Ling, Tim Dockhorn, Seung Wook Kim, Sanja Fidler, and Karsten Kreis. Align your latents: High-resolution video synthesis with latent diffusion models. In Proceedings of the IEEE/CVF conference on computer vision and pattern recognition, pages 22563–22575, 2023.
- [7] Di Chen, Yu Liu, Lianghua Huang, Bin Wang, and Pan Pan. Geoaug: Data augmentation for few-shot nerf with geometry constraints. In *European Conference on Computer Vision*, pages 322–337. Springer, 2022.
- [8] Shenchang Eric Chen and Lance Williams. View interpolation for image synthesis. In *Proceedings of the 20th Annual Conference on Computer Graphics and Interactive Techniques*, SIGGRAPH '93, page 279–288. Association for Computing Machinery, 1993.
- [9] Yuedong Chen, Chuanxia Zheng, Haofei Xu, Bohan Zhuang, Andrea Vedaldi, Tat-Jen Cham, and Jianfei Cai. Mvsplat360: Feed-forward 360 scene synthesis from sparse views. 2024.
- [10] Jaeyoung Chung, Jeongtaek Oh, and Kyoung Mu Lee. Depth-regularized optimization for 3d gaussian splatting in few-shot images. In Proceedings of the IEEE/CVF Conference on Computer Vision and Pattern Recognition, pages 811–820, 2024.
- [11] Paul E. Debevec, Camillo J. Taylor, and Jitendra Malik. Modeling and rendering architecture from photographs: A hybrid geometry- and image-based approach. In *Proceedings of the 23rd Annual Conference on Computer Graphics and Interactive Techniques, SIGGRAPH 1996, New Orleans, LA, USA, August 4-9, 1996*, pages 11–20. ACM, 1996.
- [12] Kangle Deng, Andrew Liu, Jun-Yan Zhu, and Deva Ramanan. Depth-supervised nerf: Fewer views and faster training for free. In *Proceedings of the IEEE/CVF conference on computer vision and pattern recognition*, pages 12882–12891, 2022.
- [13] Antoine Guédon and Vincent Lepetit. Sugar: Surface-aligned gaussian splatting for efficient 3d mesh reconstruction and high-quality mesh rendering. In Proceedings of the IEEE/CVF Conference on Computer Vision and Pattern Recognition, pages 5354–5363, 2024.
- [14] Chen Hou, Guoqiang Wei, Yan Zeng, and Zhibo Chen. Training-free camera control for video generation. arXiv preprint arXiv:2406.10126, 2024.
- [15] Binbin Huang, Zehao Yu, Anpei Chen, Andreas Geiger, and Shenghua Gao. 2d gaussian splatting for geometrically accurate radiance fields. In *ACM SIGGRAPH 2024 conference papers*, pages 1–11, 2024.
- [16] Ajay Jain, Matthew Tancik, and Pieter Abbeel. Putting nerf on a diet: Semantically consistent few-shot view synthesis. In *Proceedings of the IEEE/CVF International Conference on Computer Vision*, pages 5885–5894, 2021.
- [17] Rasmus Jensen, Anders Dahl, George Vogiatzis, Engin Tola, and Henrik Aanæs. Large scale multi-view stereopsis evaluation. In *Proceedings of the IEEE conference on computer vision and pattern recognition*, pages 406–413, 2014.

- [18] Bernhard Kerbl, Georgios Kopanas, Thomas Leimkühler, and George Drettakis. 3d gaussian splatting for real-time radiance field rendering. ACM Trans. Graph., 42(4):139–1, 2023.
- [19] Weijie Kong, Qi Tian, Zijian Zhang, Rox Min, Zuozhuo Dai, Jin Zhou, Jiangfeng Xiong, Xin Li, Bo Wu, Jianwei Zhang, et al. Hunyuanvideo: A systematic framework for large video generative models. *arXiv* preprint arXiv:2412.03603, 2024.
- [20] Min-Seop Kwak, Jiuhn Song, and Seungryong Kim. Geconerf: Few-shot neural radiance fields via geometric consistency. arXiv preprint arXiv:2301.10941, 2023.
- [21] Marc Levoy and Pat Hanrahan. Light field rendering. In Proceedings of the 23rd Annual Conference on Computer Graphics and Interactive Techniques, SIGGRAPH '96, page 31–42. Association for Computing Machinery, 1996.
- [22] Jiahe Li, Jiawei Zhang, Xiao Bai, Jin Zheng, Xin Ning, Jun Zhou, and Lin Gu. Dngaussian: Optimizing sparse-view 3d gaussian radiance fields with global-local depth normalization. In *Proceedings of the IEEE/CVF Conference on Computer Vision and Pattern Recognition*, pages 20775–20785, 2024.
- [23] Lu Ling, Yichen Sheng, Zhi Tu, Wentian Zhao, Cheng Xin, Kun Wan, Lantao Yu, Qianyu Guo, Zixun Yu, Yawen Lu, et al. Dl3dv-10k: A large-scale scene dataset for deep learning-based 3d vision. In *Proceedings of the IEEE/CVF Conference on Computer Vision and Pattern Recognition*, pages 22160–22169, 2024.
- [24] Ruoshi Liu, Rundi Wu, Basile Van Hoorick, Pavel Tokmakov, Sergey Zakharov, and Carl Vondrick. Zero-1-to-3: Zero-shot one image to 3d object. In *Proceedings of the IEEE/CVF international conference on computer vision*, pages 9298–9309, 2023.
- [25] Xi Liu, Chaoyi Zhou, and Siyu Huang. 3dgs-enhancer: Enhancing unbounded 3d gaussian splatting with view-consistent 2d diffusion priors. In *The Thirty-eighth Annual Conference on Neural Information Processing Systems*.
- [26] Xinhang Liu, Jiaben Chen, Shiu-Hong Kao, Yu-Wing Tai, and Chi-Keung Tang. Deceptive-nerf/3dgs: Diffusion-generated pseudo-observations for high-quality sparse-view reconstruction. In *European Conference on Computer Vision*, pages 337–355. Springer, 2024.
- [27] Fan Lu, Yan Xu, Guang Chen, Hongsheng Li, Kwan-Yee Lin, and Changjun Jiang. Urban radiance field representation with deformable neural mesh primitives. In *Proceedings of the IEEE/CVF International Conference on Computer Vision*, pages 465–476, 2023.
- [28] Tao Lu, Mulin Yu, Linning Xu, Yuanbo Xiangli, Limin Wang, Dahua Lin, and Bo Dai. Scaffold-gs: Structured 3d gaussians for view-adaptive rendering. In *Proceedings of the IEEE/CVF Conference on Computer Vision and Pattern Recognition*, pages 20654–20664, 2024.
- [29] Chenlin Meng, Yutong He, Yang Song, Jiaming Song, Jiajun Wu, Jun-Yan Zhu, and Stefano Ermon. Sdedit: Guided image synthesis and editing with stochastic differential equations. In *International Conference on Learning Representations*.
- [30] Ben Mildenhall, Pratul P Srinivasan, Rodrigo Ortiz-Cayon, Nima Khademi Kalantari, Ravi Ramamoorthi, Ren Ng, and Abhishek Kar. Local light field fusion: Practical view synthesis with prescriptive sampling guidelines. *ACM Transactions on Graphics (ToG)*, 38(4):1–14, 2019.
- [31] Ben Mildenhall, Pratul P Srinivasan, Matthew Tancik, Jonathan T Barron, Ravi Ramamoorthi, and Ren Ng. Nerf: Representing scenes as neural radiance fields for view synthesis. *Communications of the ACM*, 65(1):99–106, 2021.
- [32] Thomas Müller, Alex Evans, Christoph Schied, and Alexander Keller. Instant neural graphics primitives with a multiresolution hash encoding. *ACM transactions on graphics (TOG)*, 41(4):1–15, 2022.
- [33] Michael Niemeyer, Jonathan T Barron, Ben Mildenhall, Mehdi SM Sajjadi, Andreas Geiger, and Noha Radwan. Regnerf: Regularizing neural radiance fields for view synthesis from sparse inputs. In *Proceedings* of the IEEE/CVF conference on computer vision and pattern recognition, pages 5480–5490, 2022.
- [34] Avinash Paliwal, Wei Ye, Jinhui Xiong, Dmytro Kotovenko, Rakesh Ranjan, Vikas Chandra, and Nima Khademi Kalantari. Coherentgs: Sparse novel view synthesis with coherent 3d gaussians. In *European Conference on Computer Vision*, pages 19–37. Springer, 2025.
- [35] Ben Poole, Ajay Jain, Jonathan T. Barron, and Ben Mildenhall. Dreamfusion: Text-to-3d using 2d diffusion. arXiv, 2022.

- [36] Alec Radford, Jong Wook Kim, Chris Hallacy, Aditya Ramesh, Gabriel Goh, Sandhini Agarwal, Girish Sastry, Amanda Askell, Pamela Mishkin, Jack Clark, et al. Learning transferable visual models from natural language supervision. In *International conference on machine learning*, pages 8748–8763. PmLR, 2021.
- [37] Seunghyeon Seo, Yeonjin Chang, and Nojun Kwak. Flipnerf: Flipped reflection rays for few-shot novel view synthesis. In *Proceedings of the IEEE/CVF International Conference on Computer Vision*, pages 22883–22893, 2023.
- [38] Brandon Smart, Chuanxia Zheng, Iro Laina, and Victor Adrian Prisacariu. Splatt3r: Zero-shot gaussian splatting from uncalibrated image pairs. 2024.
- [39] Nagabhushan Somraj, Adithyan Karanayil, and Rajiv Soundararajan. Simplenerf: Regularizing sparse input neural radiance fields with simpler solutions. In SIGGRAPH Asia 2023 Conference Papers, pages 1–11, 2023.
- [40] Nagabhushan Somraj and Rajiv Soundararajan. ViP-NeRF: Visibility prior for sparse input neural radiance fields. August 2023.
- [41] Yang Song, Jascha Sohl-Dickstein, Diederik P Kingma, Abhishek Kumar, Stefano Ermon, and Ben Poole. Score-based generative modeling through stochastic differential equations. In *International Conference on Learning Representations*.
- [42] Justus Thies, Michael Zollhöfer, and Matthias Nießner. Deferred neural rendering: Image synthesis using neural textures. *Acm Transactions on Graphics (TOG)*, 38(4):1–12, 2019.
- [43] Prune Truong, Marie-Julie Rakotosaona, Fabian Manhardt, and Federico Tombari. Sparf: Neural radiance fields from sparse and noisy poses. In *Proceedings of the IEEE/CVF Conference on Computer Vision and Pattern Recognition*, pages 4190–4200, 2023.
- [44] Richard Tucker and Noah Snavely. Single-view view synthesis with multiplane images. In *The IEEE Conference on Computer Vision and Pattern Recognition (CVPR)*, June 2020.
- [45] Ang Wang, Baole Ai, Bin Wen, Chaojie Mao, Chen-Wei Xie, Di Chen, Feiwu Yu, Haiming Zhao, Jianxiao Yang, Jianyuan Zeng, Jiayu Wang, Jingfeng Zhang, Jingren Zhou, Jinkai Wang, Jixuan Chen, Kai Zhu, Kang Zhao, Keyu Yan, Lianghua Huang, Mengyang Feng, Ningyi Zhang, Pandeng Li, Pingyu Wu, Ruihang Chu, Ruili Feng, Shiwei Zhang, Siyang Sun, Tao Fang, Tianxing Wang, Tianyi Gui, Tingyu Weng, Tong Shen, Wei Lin, Wei Wang, Wei Wang, Wenmeng Zhou, Wente Wang, Wenting Shen, Wenyuan Yu, Xianzhong Shi, Xiaoming Huang, Xin Xu, Yan Kou, Yangyu Lv, Yifei Li, Yijing Liu, Yiming Wang, Yingya Zhang, Yitong Huang, Yong Li, You Wu, Yu Liu, Yulin Pan, Yun Zheng, Yuntao Hong, Yupeng Shi, Yutong Feng, Zeyinzi Jiang, Zhen Han, Zhi-Fan Wu, and Ziyu Liu. Wan: Open and advanced large-scale video generative models. arXiv preprint arXiv:2503.20314, 2025.
- [46] Guangcong Wang, Zhaoxi Chen, Chen Change Loy, and Ziwei Liu. Sparsenerf: Distilling depth ranking for few-shot novel view synthesis. In *Proceedings of the IEEE/CVF international conference on computer vision*, pages 9065–9076, 2023.
- [47] Qisen Wang, Yifan Zhao, Jiawei Ma, and Jia Li. How to use diffusion priors under sparse views? Advances in Neural Information Processing Systems, 37:30394–30424, 2025.
- [48] Shuzhe Wang, Vincent Leroy, Yohann Cabon, Boris Chidlovskii, and Jerome Revaud. Dust3r: Geometric 3d vision made easy. In *Proceedings of the IEEE/CVF Conference on Computer Vision and Pattern Recognition*, pages 20697–20709, 2024.
- [49] Zhouxia Wang, Ziyang Yuan, Xintao Wang, Yaowei Li, Tianshui Chen, Menghan Xia, Ping Luo, and Ying Shan. Motionctrl: A unified and flexible motion controller for video generation. In ACM SIGGRAPH 2024 Conference Papers, pages 1–11, 2024.
- [50] Rundi Wu, Ben Mildenhall, Philipp Henzler, Keunhong Park, Ruiqi Gao, Daniel Watson, Pratul P Srinivasan, Dor Verbin, Jonathan T Barron, Ben Poole, et al. Reconfusion: 3d reconstruction with diffusion priors. In *Proceedings of the IEEE/CVF Conference on Computer Vision and Pattern Recognition*, pages 21551–21561, 2024.
- [51] Jamie Wynn and Daniyar Turmukhambetov. Diffusionerf: Regularizing neural radiance fields with denoising diffusion models. In *Proceedings of the IEEE/CVF Conference on Computer Vision and Pattern Recognition*, pages 4180–4189, 2023.
- [52] Haolin Xiong, Sairisheek Muttukuru, Rishi Upadhyay, Pradyumna Chari, and Achuta Kadambi. Sparsegs: Real-time 360 {\deg} sparse view synthesis using gaussian splatting. arXiv preprint arXiv:2312.00206, 2023.

- [53] Sihan Xu, Yidong Huang, Jiayi Pan, Ziqiao Ma, and Joyce Chai. Inversion-free image editing with language-guided diffusion models. In Proceedings of the IEEE/CVF Conference on Computer Vision and Pattern Recognition, pages 9452–9461, 2024.
- [54] Jiawei Yang, Marco Pavone, and Yue Wang. Freenerf: Improving few-shot neural rendering with free frequency regularization. In *Proceedings of the IEEE/CVF conference on computer vision and pattern* recognition, pages 8254–8263, 2023.
- [55] Zhuoyi Yang, Jiayan Teng, Wendi Zheng, Ming Ding, Shiyu Huang, Jiazheng Xu, Yuanming Yang, Wenyi Hong, Xiaohan Zhang, Guanyu Feng, et al. Cogvideox: Text-to-video diffusion models with an expert transformer. arXiv preprint arXiv:2408.06072, 2024.
- [56] Ruihong Yin, Vladimir Yugay, Yue Li, Sezer Karaoglu, and Theo Gevers. Fewviewgs: Gaussian splatting with few view matching and multi-stage training. arXiv preprint arXiv:2411.02229, 2024.
- [57] Meng You, Zhiyu Zhu, Hui Liu, and Junhui Hou. Nvs-solver: Video diffusion model as zero-shot novel view synthesizer. *arXiv preprint arXiv:2405.15364*, 2024.
- [58] Alex Yu, Vickie Ye, Matthew Tancik, and Angjoo Kanazawa. pixelnerf: Neural radiance fields from one or few images. In Proceedings of the IEEE/CVF conference on computer vision and pattern recognition, pages 4578–4587, 2021.
- [59] Jiwen Yu, Yinhuai Wang, Chen Zhao, Bernard Ghanem, and Jian Zhang. Freedom: Training-free energy-guided conditional diffusion model. In *Proceedings of the IEEE/CVF International Conference on Computer Vision*, pages 23174–23184, 2023.
- [60] Wangbo Yu, Jinbo Xing, Li Yuan, Wenbo Hu, Xiaoyu Li, Zhipeng Huang, Xiangjun Gao, Tien-Tsin Wong, Ying Shan, and Yonghong Tian. Viewcrafter: Taming video diffusion models for high-fidelity novel view synthesis. arXiv preprint arXiv:2409.02048, 2024.
- [61] Zehao Yu, Anpei Chen, Binbin Huang, Torsten Sattler, and Andreas Geiger. Mip-splatting: Alias-free 3d gaussian splatting. In Proceedings of the IEEE/CVF Conference on Computer Vision and Pattern Recognition, pages 19447–19456, 2024.
- [62] Junyi Zhang, Charles Herrmann, Junhwa Hur, Varun Jampani, Trevor Darrell, Forrester Cole, Deqing Sun, and Ming-Hsuan Yang. Monst3r: A simple approach for estimating geometry in the presence of motion. arXiv preprint arxiv:2410.03825, 2024.
- [63] Kai Zhang, Gernot Riegler, Noah Snavely, and Vladlen Koltun. Nerf++: Analyzing and improving neural radiance fields. arXiv preprint arXiv:2010.07492, 2020.
- [64] Richard Zhang, Phillip Isola, Alexei A Efros, Eli Shechtman, and Oliver Wang. The unreasonable effectiveness of deep features as a perceptual metric. In CVPR, 2018.
- [65] Yingji Zhong, Zhihao Li, Dave Zhenyu Chen, Lanqing Hong, and Dan Xu. Taming video diffusion prior with scene-grounding guidance for 3d gaussian splatting from sparse inputs. arXiv preprint arXiv:2503.05082, 2025.
- [66] Tinghui Zhou, Richard Tucker, John Flynn, Graham Fyffe, and Noah Snavely. Stereo magnification: Learning view synthesis using multiplane images. *arXiv* preprint arXiv:1805.09817, 2018.
- [67] Zehao Zhu, Zhiwen Fan, Yifan Jiang, and Zhangyang Wang. Fsgs: Real-time few-shot view synthesis using gaussian splatting. In *European conference on computer vision*, pages 145–163. Springer, 2025.